

The Day-After-Tomorrow: On the Performance of Radio Fingerprinting over Time

Saeif Alhazbi*, Savio Sciancalepore[†], Gabriele Oligeri*

* Division of Information and Computing Technology (ICT), College of Science and Engineering (CSE), Hamad
Bin Khalifa University (HBKU), Doha, Qatar
{salhazbi, goligeri}@hbku.edu.qa

[†] Eindhoven University of Technology, Eindhoven, Netherlands
s.sciancalepore@tue.nl

Abstract—The performance of Radio Frequency (RF) fingerprinting techniques is negatively impacted when the training data is not temporally close to the testing data. This can limit the practical implementation of physical-layer authentication solutions. To circumvent this problem, current solutions involve collecting training and testing datasets at close time intervals—this being detrimental to the real-life deployment of any physical-layer authentication solution. We refer to this issue as the Day-After-Tomorrow (DAT) effect, being widely attributed to the temporal variability of the wireless channel, which masks the physical-layer features of the transmitter, thus impairing the fingerprinting process.

In this work, we investigate the DAT effect shedding light on its root causes. Our results refute previous knowledge by demonstrating that the DAT effect is not solely caused by the variability of the wireless channel. Instead, we prove that it is also due to the power-cycling of the radios, i.e., the turning off and on of the radios between the collection of training and testing data. We show that state-of-the-art RF fingerprinting solutions double their performance when the devices under test are not power-cycled, i.e., the accuracy increases from about 0.5 to about 1 in a controlled scenario.

Finally, we propose a new technique to mitigate the DAT effect in real-world scenarios. Our experimental results show a significant improvement in accuracy, from approximately 0.45 to 0.85. Additionally, our solution reduces the variance of the results, making the overall performance more reliable.

Index Terms—Physical-Layer Security; Authentication; I-Q Data.

I. INTRODUCTION

Radio Frequency (RF) fingerprinting techniques have attracted the attention of researchers working in the wireless security domain, as a way of authenticating wireless transmitters through the identification of unique patterns from the received signals [1]. Indeed, RF fingerprinting promises an effective and efficient way to authenticate the transmitting source without involving any crypto technique, thus being particularly suitable for scenarios where devices are characterized by strict battery constraints and high exposure to spoofing attacks. The transmitter does not require any additional computation or transmission, while the authentication process is completely offloaded to the receiver side, i.e., the receiver matches a pre-trained model of known transmitters to patterns extracted

from the received signals, thus being able to authenticate the source. Such patterns are indeed unique, being the side-effect of unwanted and unpredictable phenomena such as manufacturing inaccuracies during the production process at the sub-millimetre level and electronic components' impurities. Such (small) differences eventually affect the radio signals, becoming detectable by receivers that combine Software-Defined Radio (SDR) capabilities with advanced Artificial Intelligence (AI) tools, such as the ones based on Machine Learning (ML) and Deep Learning (DL) [2].

At the time of this writing, massive research is available on RF fingerprinting. Some of the contributions focused on wireless communication technologies such as LTE [3], WiFi [4], Zigbee [5], Bluetooth [6], LoRa [7], and ADS-B [8], to name a few. Other works investigated the suitability of several AI-based techniques for addressing the RF fingerprinting problem, either re-adapting well-known neural networks or casting ad-hoc solutions tailored to the specific technologies and data [9], [10], [11]. At the same time, a few works highlighted reliability issues pointing out phenomena that prevent the real-life deployment of such techniques. These works include the challenges of carrying out reliable training [12], use of multiple customized signal processing techniques by the devices under test [13], nonlinear characteristics of the power amplifiers making the fingerprint unpredictably dependant on the transmission power [14], interplay with heat dissipation, operations in different temperature conditions [15], ageing of the devices and, last but not least, variable channel conditions [16].

In this context, a few recent authoritative scientific contributions such as [16] and [12] found that training RF fingerprinting models on one day and testing on another day produces very poor performance, with a drop in the achieved classification accuracy of about 0.5. In this paper, we refer to such a phenomenon as the Day-After-Tomorrow (DAT) effect. Note that such studies adopt state-of-the-art classifiers based on the Convolutional Neural Network (CNN) *Resnet-50*, re-adapted to accept raw physical-layer signals (i.e., I-Q samples) as the input sequence, where the considered input size was either $N \times 1$ or $N \times 2$, being N the size of the input layer of the CNN. The authors of the cited studies, as well as the

wider community working on RF fingerprinting, attribute the observed performance drop to abrupt changes in the conditions of the wireless channel, masking and changing, at the same time, the unique features of the transmitter, thus calling for future research.

Contribution. In this paper, we provide several contributions. First, we reproduce the DAT effect in the same setup of previous works, while we identify and expose another root cause of the performance loss behind the DAT effect itself by considering several experiments in different wired and wireless scenarios. Although our analysis confirms that channel impairments affect classification accuracy, we prove that the measurement methodology has also a significant impact on performance. Specifically, we show that the radio's power-cycle, i.e., switching on and off the radio, significantly affects the classification accuracy when training and testing are performed on datasets collected before and after the power-cycle of the radio itself. We verified our assumptions with a wired link between the transmitter and the receiver, thus excluding all the phenomena associated with radio channel variability.

Subsequently, we consider a wireless link running for several days, and propose a new methodology to mitigate the DAT effect, exploiting the pre-processing of the I-Q samples. Inspired by recent results in the area, we refined the technique of converting the I-Q samples into images, achieving accuracy values that are (on average) twice better than the ones experienced with raw I-Q samples, while halving the variability associated with the reported accuracy. The data used for our analysis are available on request.

Roadmap. The paper is organized as follows. Section II reviews some related work on the robustness of RF fingerprinting, Sec. III introduces preliminary concepts, Sec. IV provides the details of our measurement campaign, Sec. V provides an in-depth analysis of the DAT effect describing the impact of radio power-cycle behind it. We also propose a pre-processing technique applying to the I-Q samples to mitigate the DAT effect when the power-cycle is strictly required. Section VI summarizes our findings and limitations and, finally, Sec. VII concludes the paper and outlines future work.

II. RELATED WORK

RF fingerprinting strategies include a set of techniques for identifying and authenticating RF devices by leveraging distinctive patterns in the emitted signals [2]. Such patterns originate from hardware imperfections of the devices, introduced during the manufacturing processes. In the early stage, research on RF fingerprinting focused primarily on developing custom feature extraction methods using ML and DL techniques, as shown by [17], [18], [19], [20], and [21], to name a few. Although significant progress has been achieved in the development of highly accurate methods for extracting RF features from over-the-air signals, the deployment of RF fingerprinting systems in the real world faces many challenges. One major limitation of RF fingerprinting systems based on DL algorithms is their sensitivity to wireless channel variability, which can negatively impact their performance.

Such an issue has been reported in several studies [16], where the authors found that training a DL model on data collected in one day and then testing it on data gathered in a different day significantly reduces the corresponding classification accuracy. In their experiment, the authors trained three DL models on a dataset of 20 wireless transmitters collected over several days in different environmental settings, including a cable, an anechoic chamber, and in the wild. They showed that the performance of the models was not consistent across different days, indicating that the models were not able to generalize well to new environments or conditions. These findings were corroborated by the work of the authors in [22], which also found that changing the receiver used to collect the RF signals during training can further degrade the performance of the models. Such findings highlight that the final captured RF fingerprint is a combination of three distinct factors: the transmitter's emitted signal, the channel, and the receiver's hardware. The authors in [23] studied the sensitivity of RF fingerprinting systems for LoRa networks in a wide range of scenarios, including indoor and outdoor environments, wired and wireless setups, various distances, configurations, hardware receivers, and locations. In line with previous research, they found that testing on different days and using different receivers can significantly impact the accuracy of the RF fingerprinting process. Furthermore, they observed that the variability of the protocol configuration and location also has notable effects on the achievable classification accuracy. To address the cited challenges, several mitigation techniques have been proposed in the literature. One approach is to augment the training data by exposing the fingerprinting process to a variety of channel conditions and environments, as demonstrated in [24], [25], [7], [26]. Another approach leverages the idea of injecting unique impairments to the transmitted signal such as in [18], [27], [28]. Other methods involve using channel modelling and simulations, as in [29], or using digital signal processing techniques with specialized filters, as in [30], [31]. However, none of these works provide an in-depth analysis of the DAT effect; indeed, they do not consider the impact of radio power-cycle on radio fingerprinting and they do not provide any specific solution that can deal with a real deployment. Indeed, although RF fingerprinting is a promising technique for authenticating RF devices at the PHY layer, it still faces many limitations and challenges. In this work, we push further the analysis of the performance of the RF fingerprinting in real-world scenarios by shedding light on root causes that affect its performance.

III. PRELIMINARIES

In this section, we introduce the adopted hardware and software setup and the required background concepts related to RF communication and DL for radio fingerprinting.

Hardware Set-up. The hardware considered in this paper includes seven (7) SDRs USRP X310 [32], featuring the UBX160 daughterboard and the VERT900 antenna [33]. The general setup is depicted in Fig. 1, showing that the radios are connected to two laptops HP EliteBook I7, featuring 32GB of RAM. All the considered scenarios involve radio 1 (the one

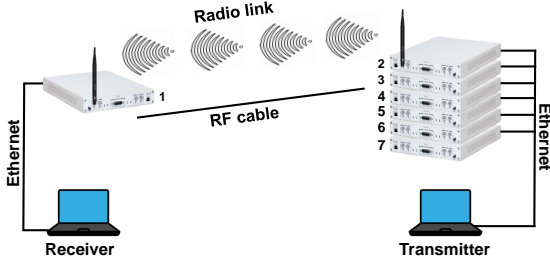


Fig. 1: Hardware setup: our measurement setup consists of 1 receiver and 6 transmitters communicating via either a wireless or a wired link, depending on the scenario.

on the left side in Fig. 1) as the receiver, while we consider the other ones as the transmitters (only one active for each experiment). Depending on the specific measurement scenario, the transmitter and the receiver have been connected via either an RF (wireless) or a wired link. In the former, we considered a transmitting power of 35mW and a normalized receiver gain of 1, while when using a wired link we set the transmission power to 1 mW and the normalized receiver gain to 0.8, where the normalized receiver gain is defined according to the logic in the USRP Source block provided by GNURadio (see software setup below). Finally, for the wired link, we considered a coaxial cable type RG58A/U. We do note that other works in the RF fingerprinting research area might consider a higher number of transmitter radios. However, our findings confirm their performance, while paving the way for future research in the areas.

Software Setup. We adopted GNURadio v3.8 for the measurements, by defining a transmission chain made up of the following blocks:

- *File source.* We generated a message including a string of 256 bytes with incremental value, i.e., $[0, \dots, 255]$. Note that specifying a valid message is necessary to draw any conclusions on the effectiveness of the TX-RX chain, as well as on the bit-error rate experienced by the communication link.
- *Constellation modulator.* We configured the modulator according to the Binary Phase Shift Keying (BPSK) modulation.
- *UHD: USRP Sink.* We configured the transmitter to work at the frequency 900 MHz, with a sample rate of 1M samples per second, and finally, transmission power of either 35mW or 1mW for the wireless and the wired link, respectively.

We configured the receiver according to the following chain:

- *UHD: USRP Source.* We tuned the receiver to the reference frequency of 900 MHz, with a sample rate of 1M samples per second, and a normalized receiver gain of either 1 or 0.8 depending on the adopted link, being wireless or wired, respectively. Note that, when transmitting complex I-Q values, the modified Nyquist

theorem requires that the sample rate at the receiver should be at least equal (or higher) than the sample rate at the transmitter [34].

- *AGC.* We included the Adaptive Gain Control block to mitigate channel fluctuations.
- *Symbol Sync.* We included a symbol synchronizer to receive and decode digital signals based on the maximum likelihood estimation (mle) criterion.
- *Costas Loop.* We adopted the Costas loop to mitigate the phase offset and residual frequency offsets.
- *File Sink.* The output of the receiving chain is stored inside a file, for follow-up analysis.

I-Q Samples. Given the carrier frequency f_0 , which in our case is 900 MHz, a digital modulation scheme can be described through Eq. 1 [35].

$$x(t) = I \cos(2\pi f_0 t) + Q \sin(2\pi f_0 t), \quad (1)$$

where $x(t)$ is the transmitted modulated signal, I is the *in-phase* component, while Q is the *quadrature* component. For the specific modulation scheme considered in this work, i.e., BPSK, the quadrature component always has a null value ($Q = 0$), while the in-phase component is used to translate the value of the bit b , i.e., $I = -1$ and $Q = 0$ when $b = 0$, and $I = +1$ and $Q = 0$ when $b = 1$, or vice-versa, as shown by Eq. 2.

$$x(t) = \begin{cases} +1 \cos(2\pi f_0 t), & \text{if } b == 1 \\ -1 \cos(2\pi f_0 t), & \text{if } b == 0 \end{cases} \\ = \cos(2\pi f_0 t + \phi), \quad (2)$$

where ϕ takes on the value of either 0 or π as a function of the value of the bit. Since I and Q constitute an alternative way to represent the magnitude and phase of the modulated signal $x(t)$, it is natural to consider the I and Q components as the real and imaginary parts of a complex number, respectively. In particular, for the BPSK, there is no imaginary part ($Q = 0$), while we only consider the real component, i.e., $I = \pm 1$. Given a sequence of bits, the transmitter implements Eq. 2 to translate bits into I-Q samples, while the receiver takes on the challenge to reverse each I-Q sample to the original value of the bit. As a toy example, we consider Fig. 2, representing a sequence of I-Q samples over time. The measurement consists of 8000 I-Q samples (black dots) collected by using a wired link between the transmitter and the receiver, while the red lines and the associated red dots (at the end of the lines) represent the theoretical (ideal) position of the I-Q samples, i.e., $[1, 0]$ and $[-1, 0]$. Due to radios imperfections, the I-Q samples spread over the I-Q plane with a specific pattern peculiar to the adopted combination of transmitter and receiver radios. Finally, we report the projection of the I-Q samples at the bottom of the figure to provide a more concrete representation of the actual spreading of the I-Q samples, i.e. the *radio fingerprint*.

Deep Learning. We denote *radio fingerprinting* as the task of identifying unique features at the physical-layer (I-Q samples) that can be used to discriminate a radio transmitter. A radio fingerprint is a unique pattern in the I-Q samples, like the one depicted in Fig. 2. Many researchers have undertaken the challenge of identifying a robust fingerprint and developing

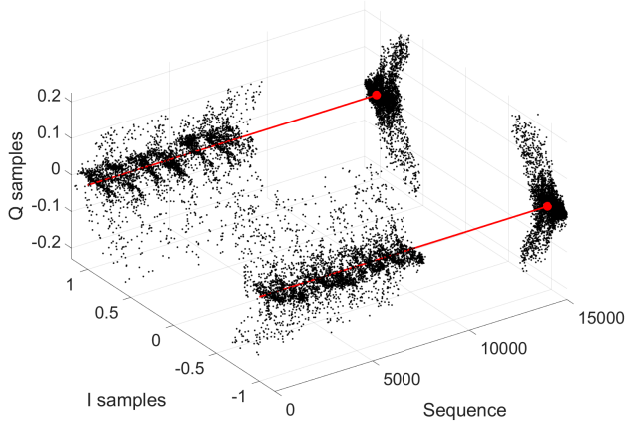


Fig. 2: I-Q samples: solid red lines represent the theoretical position of the I-Q samples for a BPSK modulation scheme, i.e., $[-1, 0]$ and $[1, 0]$, while the dispersion of their values is mainly caused by the transducers’ imperfections—these samples are coming from a wired measurement—thus representing the fingerprint of the radio.

a methodology to use it efficiently and effectively. State-of-the-art solutions involve a two-stage process: (i) *training* a neural network model with chunks of I-Q samples, and (ii) *testing* a sequence (of I-Q samples) from the wild to identify the actual transmitter. Among the several neural networks proposed in the literature, the family of Residual Neural Networks (RNN) emerged as a good trade-off between training speed and classification performance. In particular, *resnet50* is the one adopted in this work, in line with other authoritative related works (see Sec. II). In the remainder of this manuscript, we consider the *resnet50* implemented in MatLab R2022b®, constituted by 50 layers and pre-trained on the ImageNet database. The neural network, as it is originally designed, cannot be used for the training and classification of the I-Q samples, and researchers developed different ways to modify it to fit the radio fingerprinting problem. Indeed, *resnet50* is designed to classify images from the ImageNet dataset—thus requiring some modifications both at the input and at the output layers. The input layer is usually adapted to fit raw I-Q samples (and not images), while the output layer is changed to fit the number of transmitters—being different from the 1000 classes of ImageNet. Moreover, the network itself is already trained to classify images such as dogs, cats, flowers, etc.—these being different from the input adopted for the RF fingerprinting; therefore, the network requires a partial re-train to expose the model to the new input.

In detail, the output layers (*fullyConnectedLayer* and *classificationLayer*) should be re-adapted to take into account the number of classes in the radio fingerprinting problem, i.e., the number of radio transmitters to identify. As for the input layers, two main configurations have been considered: (i) input of interleaved raw I-Q samples consisting of a vector of dimensions either $N \times 1 \times 1$, as in [16], or $N \times 2 \times 1$, as

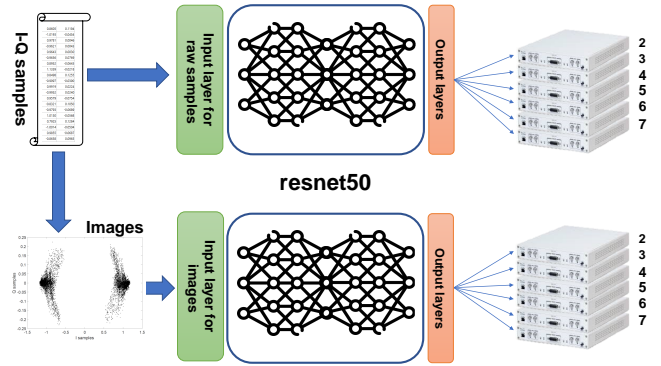


Fig. 3: The classification process for RF fingerprinting: a neural network (*resnet50*) is re-adapted to fit either raw I-Q samples or images (input layers) and to identify the correct number of radios (output layers).

in [12], and (ii) images where the input is a matrix of size $224 \times 224 \times 3$, where 224×224 is the size of the images in the ImageNet dataset, as in [36].

In the remainder of this paper, we will consider both the approaches of raw I-Q samples and images, to compare the performance and highlight their limitations. Figure 3 shows how we deployed *resnet50* to identify the transmitter given the I-Q samples collected by the receiver, considering the pre-processing approaches discussed above.

IV. MEASUREMENT COLLECTION

We define *measurement* a continuous flow of I-Q samples between the transmitter and the receiver. As will be clarified in the following, we consider two types of measurements: (i) short measurements lasting 300 seconds (5 minutes) and (ii) long-term measurements lasting for 4 days. In the remainder of this work, we refer to I-Q samples as complex-valued data; thus, each radio sample (bit) is constituted by one I and one Q sample. Given the availability of 6 transmitters, we define *run* of measurements as the sequence of 6 consecutive measurements where the receiver is the same while the transmitter changes every time among all the available ones. Finally, we define *dataset* as a sequence of several runs of measurements. All the datasets leveraging a wireless link share the same scenario, i.e., an indoor environment where the transmitter is located 10 meters far away from the receiver, without the line-of-sight (nLoS). During our measurement campaign, we collected three datasets of measurements, listed below and summarized in Tab. I.

- 1) *Dataset 1 (DS1)*. This dataset is constituted of 78 measurements, organized in 13 runs, collected by using a wired link and power-cycling the radios (both the transmitter and the receiver) after each measurement. We kept the same receiver for all the measurements, while we changed the transmitter (using 6 different radios, in total).
- 2) *Dataset 2 (DS2)*. This dataset is constituted by 6 non-stop measurements collected by using a wired link for 3 days for each measurement ($6 \times 3 = 18$ days, 265B+

TABLE I: Measurements description: We collected three datasets over wired and wireless links, lasting multiple days.

	Link	Sample Rate [Msps]	Duration [Days]	Runs	Samples per Measurement
DS1	Wired	1	3	13	144M+
DS2	Wired	0.256	18	1	33B+
DS3	Radio	1	4	12	144M+

samples). All the measurements share the same receiver while we changed the transmitters (using 6 different radios in total, as for the previous dataset). Given the duration of the measurements, we had to decrease the sample rate to 256K samples per second.

- 3) *Dataset 3 (DS3)*. This dataset is constituted by 72 measurements, collected using the wireless radio link (using the carrier frequency $f = 900$ Mhz) in an indoor environment, with people moving around, over 4 days with a distance between the transmitter and the receiver of 10 meters. For each day, we collected 3 runs of measurements (6 measures each) early in the morning, noon, and late evening. To be consistent with the other measurements, we considered the same radio as the receiver, while we swapped the transmitters among the 6 available radios.

Note that we consider multiple transmitters, but only a single receiver. This is done on purpose to replicate the traditional setup adopted in the literature for RF fingerprinting. Analyzing the impact of a different receiver on the performance of RF fingerprinting solutions is out of the scope of this contribution, as well as part of our future work.

V. THE DAY-AFTER-TOMORROW EFFECT

In this section, we first summarize the methodology followed in our investigation (Sec. V-A), and subsequently, we provide an in-depth analysis of the DAT effect (Sec. V-B). Moreover, in Sec. V-C, we introduce a mitigation technique for the DAT effect leveraging the pre-processing of I-Q samples into images and, finally, in Sec. V-D, we deploy our solution to a real wireless radio link.

In the following, we use the qualitative terms *low* and *high* associated with the accuracy of the classifier just for the sake of simplicity, as well as to introduce the problem tackled in our manuscript. A quantitative analysis of the phenomena involving real measurements, taken with both wireless and wired links, will be presented in the subsequent sections to support our claims.

A. Methodology

This section discusses the *Day-After-Tomorrow* effect, i.e., a common problem affecting all the approaches dealing with RF fingerprinting presented in the literature and mentioned explicitly in some of them, e.g., [16] and [12]. We describe the phenomenon through real measurements, whose logic is depicted in Fig. 4 using two experiments (E1 and E2). We highlight that experiments E1 and E2 depict a radio link but, in the following, we might consider either a wireless or a

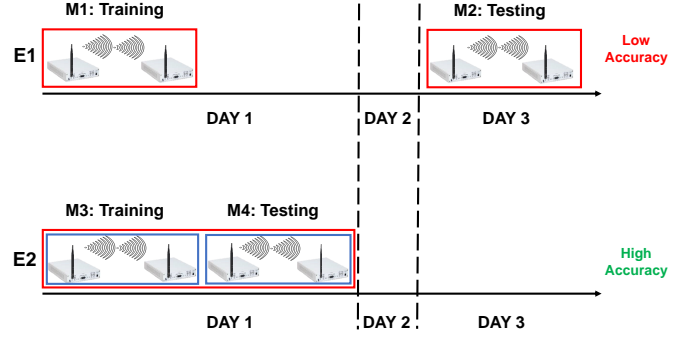


Fig. 4: The *Day-After-Tomorrow* effect is constituted by two experiments (E1 and E2): training a model on a measurement (M1) taken one day (DAY 1), and then, testing on a measurement (M2) taken on another day (DAY 3) gives low accuracy performance. Conversely, training and testing on chunks (M3 and M4) taken from the same measurement (DAY 1) gives high accuracy performance.

wired link, depending on the objectives of the experiments. For both experiments (E1 and E2), two measurements (red boxes) are collected. During the first experiment (E1), the measurements (M1 and M2) are taken on two different days (Day 1 and Day 3). In contrast, during the second experiment (E2), only one measurement is taken (one red box) and then split into two chunks (blue boxes), M3 and M4 respectively, taken on Day 1 without interrupting the measurement process. For both experiments, we use one measurement to train a neural network model, i.e., M1 in E1 and M3 in E2, while we consider the second measurement for testing, i.e., M2 in E1 and M4 in E2.

We refer to the *Day-After-Tomorrow* (DAT) effect as the phenomenon where the first experiment E1 is characterized by a low classification accuracy compared to the second experiment E2, which experiences a high classification accuracy. This is a well-known effect in the literature, reported by recent authoritative contributions such as [16] and [12], to name a few. Such works explain the DAT effect by referring to the unpredictability of the wireless radio channel and its associated phenomena, e.g., multipath and fading. We highlight that the DAT effect significantly hinders the deployment of radio fingerprinting techniques in any real-world scenarios since the model trained at a specific time cannot be effectively re-used in the future without reporting significant performance loss. While we acknowledge the impact of the radio channel in the fingerprinting process, in the following, we formulate a different hypothesis rooted in real experiments involving both wireless and wired links. Our intuition is that the loss of performance described above is not caused by the channel variations only—although the channel might play an important role—but by another phenomenon, i.e., the *power-cycle* of the radios in-between the measurements used for the training and the testing tasks.

Definition 1. We define power-cycle as the process involving the software (re-)initialization of the radio. This takes place

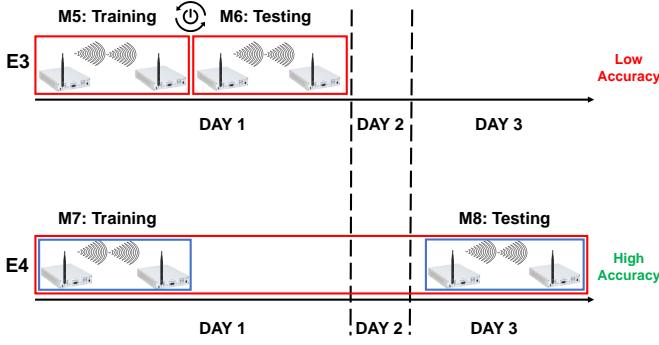


Fig. 5: The *power-cycle* problem: consecutive measurements (M5 and M6) experiencing similar channel conditions achieve low classification accuracy if radios are power-cycled in between the measurements. Conversely, a long-lasting measurement (E4) experiencing very different channel conditions achieves high accuracy if the two chunks (M7 and M8) are from the same measurement, i.e., they are not separated by a power-cycle.

by applying the power-off/power-on of the radio.

Figure 5 wraps up the experiments we made to expose the phenomenon described above. As before, we highlight that the experiments depict a radio link but in the following, we might consider either a wireless or a wired link depending on the objectives of the experiments. Specifically, we consider two additional experiments (E3 and E4): during E3, two measurements (M5 and M6) are collected by power-cycling the transmitter and the receiver in-between the measurements, i.e., switching off and on the radios. We stress that M5 and M6 are taken one immediately after the other, i.e., very close in time, by only switching off and on the radios (power-cycling). We use M5 for training and M6 for testing. We observed a low classification accuracy for both the wireless and the wired scenario. Finally, we consider another experiment (E4) constituted by a long measurement (spanning 3 consecutive days) where no power-cycle is performed in between the measurements. From this experiment, we extract two chunks, i.e., M7 and M8. When considering M7 for training and M8 for testing, the resulting classification accuracy is high.

In the following sections, we also show that it is possible to mitigate this phenomenon and significantly increase the classification accuracy for measurements separated by a power-cycle (E3). This is achieved by pre-processing the I-Q samples and converting them into images, adopting these later ones as the input to the CNN.

B. DAT: In-depth analysis

The vast majority of the literature explains the DAT effect with the unpredictability of the radio channel, by considering the changes affecting the environment surrounding the transmitter and the receiver. As an example, we consider Fig. 6, consisting of 7 sub-figures (100,000 I-Q samples each) taken from subsequent chunks in an actual radio measurement. Fig. 6(a) and (g) represent the steady state, before and after

the perturbing event, i.e., a person walking close to the radio link. It is worth noting that the I-Q samples, and therefore the transmitter’s fingerprint, are strongly affected by the considered event. This is evident by looking at the figures from Fig. 6(c) to (e), and in particular, Fig. 6(d), showing a set of I-Q samples completely different from the ones at steady state, i.e., Fig. 6(a) and (g).

Phenomena like the one in Fig. 6(d) completely change the I-Q displacement at the receiver, making the retrieval of the fingerprint (almost) impossible. When such events occur, e.g., people moving close to the transmitter-receiver link and abrupt changes in the environment, the classifier might generate a false negative—not being able to recognize the transmitter features. We acknowledge that such false negative is not due to misclassification, but to the impossibility to retrieve features that are hidden by the complete re-displacement of the I-Q samples. Nevertheless, multipath effects are not the only ones to make the RF fingerprinting process unreliable. In the following, we highlight that even *excluding the multipath*, there are measurement configurations which prevent the fingerprinting process. To discuss more in-depth the DAT effect and its causes, we consider a wired link between the radios. We consider this scenario as it excludes any dependencies on the multipath and other effects due to RF propagation while keeping the noise due to the communication channel at a minimum. We will extend our results to the RF link in Sec. V-D.

Power-cycle. We consider the dataset *DS1* (from Section IV), and we run the experiment E1. Given the 13 runs of *DS1*, we randomly choose an increasing subset of the runs for the training process (from 1 to 12) and only one run (for all the considered cases) for testing—the testing run is always mutually exclusive with respect to the runs constituting the training set. We repeated this procedure 20 times. Figure 7 shows the results of our experiments considering a CNN structure similar to the one of [16] and [12], i.e., *ResNet50*, providing as input raw I-Q samples in the form $N \times 1$.

Figure 7(a) shows the accuracy of the classifier when the training process is exposed to an increasing number of runs, i.e., from 1 to 12. For each considered number of runs in the training process, the central mark in the box plots indicates the median value, while the bottom and top edges of the box indicate the percentiles 0.25 and 0.75, respectively. The whiskers extend to the most extreme data points not considered outliers, and the outliers are plotted individually using the “+” marker symbol. The solid red line represents the mean value of the accuracy samples. The accuracy spans approx. between 0.3 and 0.6 (on average) while being characterized by a relatively high variance (≈ 0.3). These results are consistent with the ones reported in [16], where the authors considered the same scenario (wired) and a similar neural network structure. We stress that all the measurements have been taken by power-cycling the radio every time (E1). Thus, the low performance of the classifier cannot be attributed to the radio channel unpredictability—indeed, we are using a cable, attenuating the dependency on the RF channel propagation. For the sake of completeness, we report recall and precision considering the average value (solid red line), and the region comprised

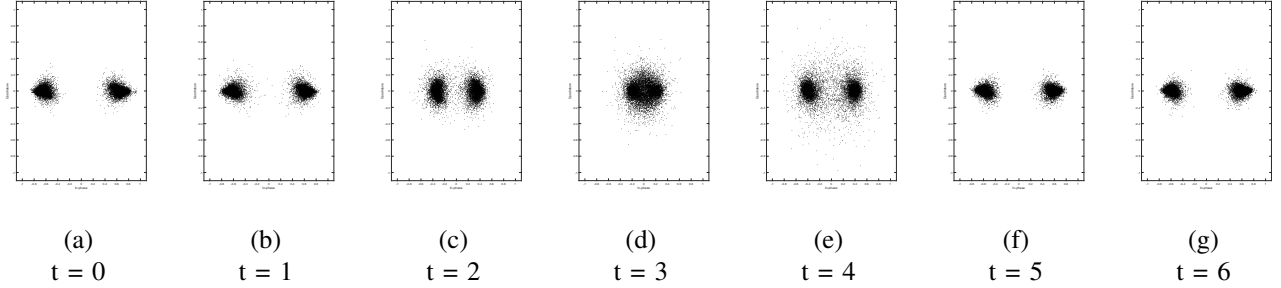


Fig. 6: The effect of people moving around close to the transmitter-receiver link across seven time windows. Compared to a static environment (Figs. (a), (b), (f), and (g)), the shape of the I-Q samples at the receiver (modulated through the BPSK scheme), is significantly affected (see Figs. (c), (d), and (e)).

between quantile 10 and 90. Finally, black circles represent the actual outcomes of each specific experiment. Finally, we highlight that Fig. 7 is also taking into account experiment E3. Indeed, since the 13 runs of *DS1* are collected over 3 days, i.e., 3 on the first day, 5 on the second one, and finally, 5 on the third one, there are high chances to have adjacent measurements (one after the other, like in E3) when considering a high number of runs, e.g., 12 runs. Thus, Fig. 7 captures two distinct phenomena: (i) when the number of runs is small, i.e., left side of the x-axis, the training and testing are likely to be performed on datasets that are temporally far away from each other (E1); and (ii) considering the right part of the x-axis, the training and testing are more and more likely to be temporally close each other (E3)—still being separated by a power-cycle. Both the experiments (E1 and E3) confirm that the power-cycle strongly affects the performance of the classifier.

No power-cycle. We now consider *DS2*, i.e., the long measurements over 3 days, and the same methodology as before. We run experiments E1 and E2 over the long measurements to investigate if the performance of the classifier is affected by either the power-cycle (absent) or the temporal distance between two chunks extracted from the measurements. To this aim, we split the 3-day measurements into 10 chunks, obtaining a total of 60 chunks. Starting from 6 measures characterized by the same receiver and 6 different transmitters (recall the general set-up from Fig. 1), we randomly selected one or more chunks (up to 9) for training and one for testing (not belonging to the training set). Figure 8 shows the accuracy (quantiles 0.25, 0.75, median, and outliers) of the classifier based on the *resnet-50* network. The differences between Fig. 7(a) and Fig. 8 are striking: given the same scenario, i.e., a wired link between the transmitter and the receiver, the different performance of the classifier are due to how the measurements have been collected. If the measurements adopted for training and testing are separated by a power-cycle, the performances of the classifier are negatively affected (Fig. 7(a)); conversely, if the training and testing datasets are not separated by a power-cycle, the fingerprint is consistent and can be identified with overwhelming probability (Fig. 8). Finally, Fig. 9 provides the normalized confusion matrix considering all the experiments performed for Fig. 8: it is worth noting that only about 1% of the samples are misclassified.

Wrap-up. Although we acknowledge that the radio channel variations affect the fingerprinting process, we showed that the power-cycling of the radio plays a major role, as well. Indeed, while common knowledge assumes that low classification accuracy is due to different channel conditions between the measurement adopted for training and the one for testing (Experiment E1 in Fig. 4), we proved that two consecutive measurements are affected by the same effect when a power-cycle is performed in-between (Experiment E3 in Fig. 5)—we observed this phenomenon by considering a wired link, so being independent of the multipath fading. Moreover, we also confute the common assumption that measurements taken during the same day (Experiment E2 in Fig. 4) do not suffer the DAT effect, due to the high correlation of the experienced radio channels. Indeed, by considering experiment E4 in Fig. 5, the two chunks (M7 and M8) are separated by a long time but still allow a high classification accuracy due to the absence of the power-cycle between M7 and M8.

C. DAT mitigation

In this section, we introduce a possible solution to mitigate the DAT effect through a dedicated pre-processing of the I-Q samples. Our intuition is rooted in the observation that raw I-Q samples are too noisy, even when considering controlled scenarios (wired). At the same time, CNNs have been created to process images, and thus their performances should be optimal when providing images as input. Therefore, we introduce a pre-processing technique that averages the spatial displacement of I-Q samples, thus mitigating the noise hiding their features. Inspired by [36], we propose a modified pre-processing technique as depicted in Fig. 10. Our methodology considers raw I-Q samples as input from the modulated signal, in this case, BPSK. The raw I-Q samples are mainly organized in two clouds, i.e., one cloud represents the bits equal to 1, while the other cloud represents the zeros—similar considerations can be extended for more complex modulation schemes. The first step consists of defining a chunk size to process the I-Q samples: we consider a chunk size equal to 100,000 I-Q samples, already taken into account in [36]. The subsequent step differentiates from the reference approach by splitting the original chunk into two chunks containing the left and right clouds, respectively. We trim each cloud and compute a bi-variate histogram, by dividing the I-Q plane into

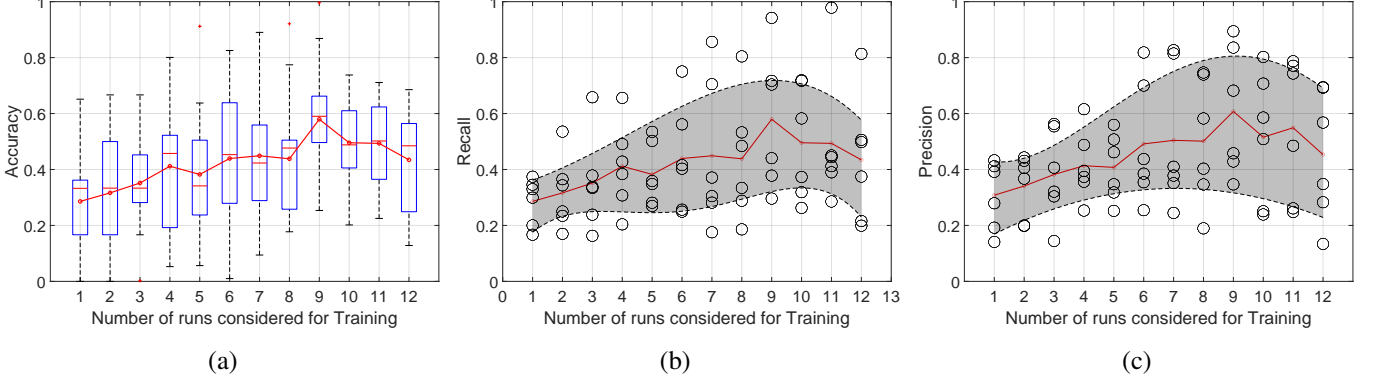


Fig. 7: Wired scenario and raw I-Q samples as input of the classifier. Accuracy (a), Recall (b) and Precision (c). The performance of the classifier refers to experiment E3, i.e. when each measurement is taken after a power-cycle of the radio.

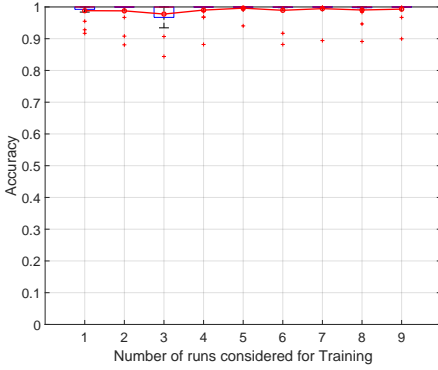


Fig. 8: Wired scenario and raw I-Q samples as input of the classifier: Accuracy as a function of the number of runs adopted for the training process. The performance of the classifier refers to experiment E4 when long measurements are taken (3 days) and no power-cycle is performed during the measurement campaign.

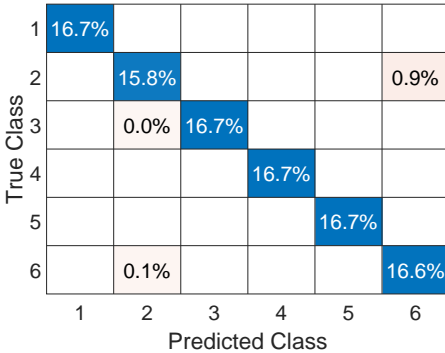


Fig. 9: Wired scenario and raw I-Q samples as input of the classifier: Confusion matrix computed over all the accuracy outcomes.

224×224 tiles (the size of the images to be used as input to the *resnet50* network). Then for each tile, we count the number of received I-Q samples. Contrary to [36], we consider three layers for the generation of the images, i.e., one layer for each primary colour component (red, green, and blue). Therefore, assuming an image as constituted by a three-layers matrix, i.e., $[224 \times 224 \times 3]$ (one layer for each primary colour), and the pixel value spanning between 0 and 255, we assign each value of the tile through the following rule.

- $0 \leq x_T \leq 255$, then $p_R = 0, p_G = 0, p_B = x_T$,
- $256 \leq x_T \leq 511$, then $p_R = 0, p_G = x_T - 255, p_B = 255$,
- $x_T > 511$, then $p_R = x_T - 510, p_G = 255, p_B = 255$,

where x_T represents the value of the tile from the bi-variate histogram, while p_R, p_G and p_B are the pixel values, i.e., red, green and blue, respectively. Finally, we observe that if $x_T > 767$, it is clipped to 767—this issue can also be controlled by properly adjusting the chunk size. Figure 10 summarizes the image generation process considering the three image's components, i.e., red, green and blue. Note that the mentioned modification compared to the solution in [36] improves the ability of the CNN to adapt to multiple power-cycles of the devices.

Power-cycle. We now reconsider the Dataset 1 (*DS1*) from Sec. IV and experiments E1 and E3 from Fig. 4 and Fig. 5, respectively. Moreover, we repeated the same experiments as we did before (Fig. 7) by only considering the different procedure presented in Fig. 10, i.e., we considered the images as input to the CNN in place of raw I-Q samples. Figure 11 shows the accuracy, recall and precision associated with our tests. We considered an increasing number of randomly chosen runs, from 1 to 12, for the training process, and we tested each configuration 20 times. For the testing, instead, we considered only one run (random and disjoint from the training set). The performance of the proposed classification methodology is much better compared to the ones of raw I-Q samples adopted by [16] (recall Fig. 7). Indeed, when training with 5 randomly chosen runs of measurements, the accuracy is higher than 0.9 while it is about 0.35 when considering raw I-Q samples. Moreover, exposing the model to more and

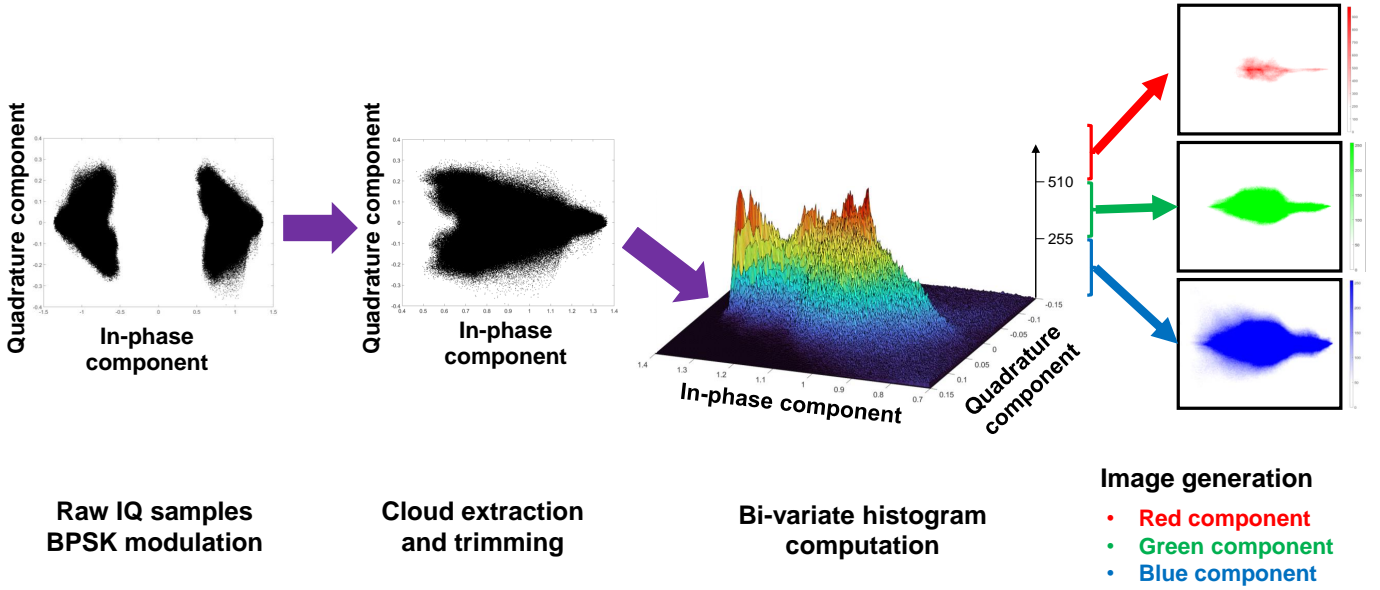


Fig. 10: Our solution to mitigate the DAT effect: I-Q samples are pre-processed to generate images.

more runs significantly increases the performance—this is not happening when considering raw I-Q samples. Finally, recall and precision metrics, reported in Figs. 11(b) and (c), confirm the quality of our proposed classification algorithm when considering false negatives and false positives, respectively.

D. Real scenario: radio link

In this section, we consider a real scenario constituted by the measurement set-up considered in Fig. 1, with a wireless link working at the frequency $f_0 = 900\text{MHz}$. In this context, we compare the performance of the classifiers considering raw I-Q samples ([16]) and images from dataset *DS2*, as described in Sec. IV. We recall that the measurements in *DS2* have been taken to expose as much as possible the DAT effect: indeed, each measurement lasts for 5 minutes and it is collected at random for 4 days, with several power-cycles in-between.

Figure 12 shows the comparison between the raw I-Q samples and the images when considering *resnet50* and dataset *DS2*. We adopted the same methodology described before, selecting from 1 to 11 runs for training and a random run for testing, disjoint from the training set. Each black circle and cross in Fig. 12 represents the outcome of a training/testing process for the images and raw I-Q samples, respectively. The shaded green and red areas refer to the quantiles 0.2 and 0.8 computed on the measured accuracy for both the images and raw I-Q samples. Finally, the solid red and green lines interpolate the accuracy outcomes from the raw I-Q samples and the images, respectively.

We observe that the performance of our proposed image-based technique outperforms the ones of raw I-Q samples, i.e., the green shaded area is always well on top of the red one, with a minor overlapping area in the region comprised between 1 and 10 runs. We also highlight the variance associated with the accuracy: raw I-Q samples are characterized by a very high variance (≈ 0.6) independently of the number of considered runs. This is a critical issue for the repeatability of the experiments when adopting raw I-Q samples: in many cases, single runs based on raw I-Q samples might experience high accuracy, e.g., higher than 0.8, leading to exceptional claims about the feasibility of using such a technique for fingerprinting. However, a systematic replication of the training/testing procedure exposes the issue of a flat (and poor) performance, which is (almost) independent of the training set size.

Images (shaded green area) behave much better. The average accuracy spans between ≈ 0.6 and ≈ 0.85 , depending on the training set size, and our results indicate that extending the training process to a higher number of runs might increase the performance even more. Moreover, we observe that the variance associated with the results is still an issue: even assuming the best configuration (high number of runs), the variance associated with the accuracy is ≈ 0.2 , although it decreases when more data is considered for training. In our vision, such a variance might be still relatively high for many real-life applications, requiring smaller confidence. At the same time, we observe that the usage of our technique based on images significantly improves the performance of the RF fingerprinting process, taking a significant step toward

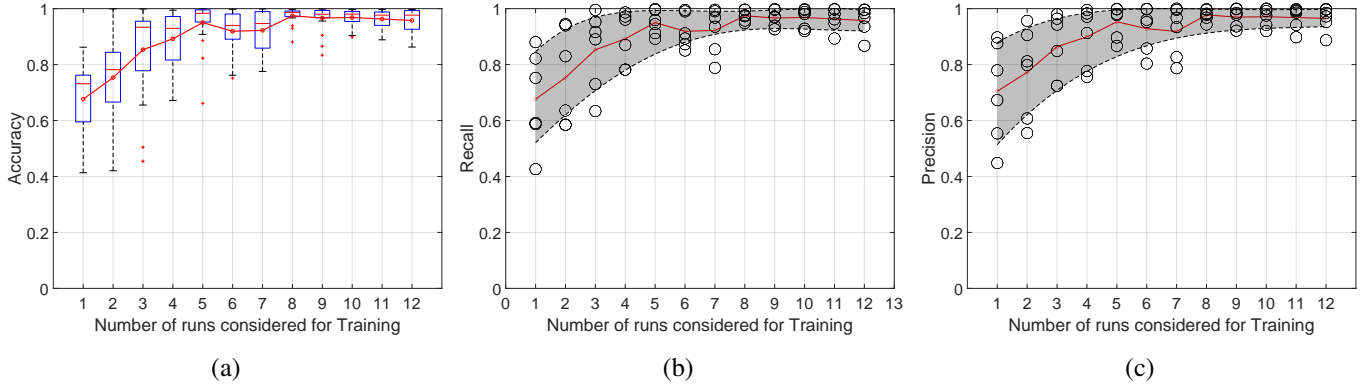


Fig. 11: Wired scenario and images as input of the classifier: Accuracy (a), Recall (b) and Precision (c).

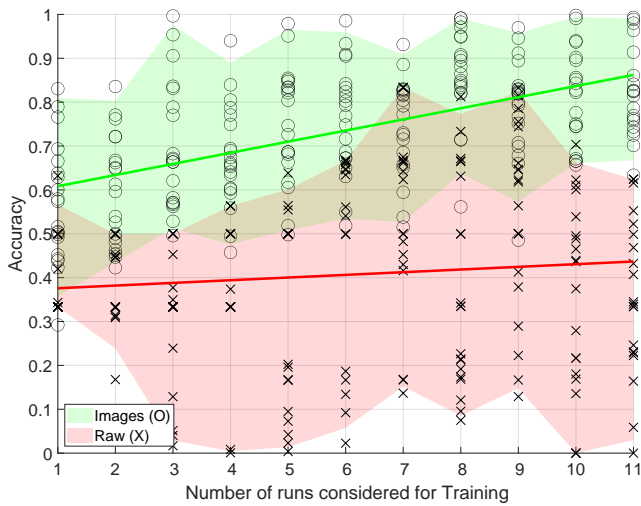


Fig. 12: Comparison of raw I-Q samples and images on measurements taken on a wireless link with power-cycle.

the deployment of RF fingerprinting techniques in the wild.

Finally, we acknowledge that the DAT effect still affects the classification process even when pre-processing I-Q samples into images. In this context, our work shows that techniques based on raw I-Q samples analysis are less robust to power-cycling, while solutions based on images generated from I-Q samples have the potential to overcome such an issue, showing promising results. Likely, other networks than the one used above (*ResNet-50*) might achieve higher performance. Thus, further research is likely required in this area to increase the accuracy while reducing the associated variance. However, to the best of our knowledge, this manuscript is the first to conduct a systematic analysis of the DAT effect and demonstrate experimentally the impact of devices' power-cycle on the accuracy of RF fingerprinting techniques.

VI. WRAP-UP AND DISCUSSION

Summary. Following the in-depth investigation described in Sec. V, the DAT effect can be re-defined and summarized as the twist of performance affecting the RF fingerprinting process when the samples used for the training and testing datasets

do not belong to the same measurement. A common (and accepted) explanation involves the wireless channel variability, i.e., different measurement times involve a different radio channel, thus causing different performance. The investigation performed in this work proves this to be a partial (and in some cases, ineffective) explanation of the problem.

Although we acknowledge the impact of channel variability, we identified the radio's power-cycle as the main cause of performance loss. Such a phenomenon is independent of the status of the radio channel and detrimental to the identification of the transmitter, also considering measurements very close in time, and thus, experiencing the same channel conditions. Although some authors already observed it (e.g., [16] and [12]), to the best of our knowledge, no one before provided a thorough analysis of the DAT effect, shedding a light on its causes and possible mitigation strategies.

In our manuscript, we first reproduced the DAT effect in a controlled scenario (a wired link between the transmitter and the receiver), by power-cycling the radios under test. Indeed, the power-cycle changes the fingerprint enough to significantly reduce the accuracy of the identification process—halving its accuracy in many cases. The DAT effect disappears when considering the same measurement set-up, but taking chunks of data from a long measurement not being affected by a power-cycle. Under this scenario, standard techniques (adopting raw I-Q samples) easily achieve accuracy close to 1. These findings show that the DAT effect exists independently of the wireless channel, bringing new insights into the current state of the art.

The causes behind the fingerprint's change are likely linked to the software re-initialization affecting the SDRs after a power-cycle. Indeed, at a high-level, SDRs involve mainly two blocks: (i) the FPGA and (ii) the radio-frequency (RF) module. The former (FPGA module) implements the network interface drivers, the data flow command and control, the decimation/interpolation, and finally, the digital up/down conversion (DUC/DDC), while the latter (RF module) implements the analogue transmission of the signal. An important intermediate block between the FPGA and the RF module performs the analogue-to-digital (ADC)/digital-to-analogue (DAC) conversion of the signal. We believe that the power-cycle might affect the internal parameters of those blocks, changing the behaviour of the radio at the physical-layer.

Interplay of DAT with other effects. Complementary causes such as the use of different signal processing techniques [13], nonlinear characteristics of power amplifiers being dependent on the average output [14], heat dissipation and the associated device temperature [15], and clock skews [37] have been already identified as hardware/software parameters that can change from one measurement to the other one. In this paper, we pushed the analysis further by clearly identifying and describing a problem which hinders the deployment of radio fingerprinting in real scenarios. Other effects, such as heat dissipation due to long run of the devices and ageing of the devices, are also likely to affect the accuracy of RF fingerprinting in the wild. Analyzing the joint effect of the phenomena mentioned above and the DAT effect on the accuracy of the RF fingerprinting process will be the immediate future step in this research.

Limitations. Our analysis involved only specific radios, i.e., USRP Ettus X310, and we cannot infer the impact of the DAT effect on other devices. Nevertheless, our analysis is in line and subsequent to the findings of the authors in [16], where they observed the same DAT phenomenon considering 20 devices constituted by USRP N210 and USRP X310. Similarly, the authors in [12] observed the phenomenon by considering the USRP B210 and 25 Pycom Lora-enabled devices. Thus, we are confident about the general validity of our results. Finally, we are confident that the DAT effect has been observed by many other researchers, but since its cause can be easily attributed to the wrong source (channel variability), it did not receive the attention it deserves.

Robustness to Spoofing Attacks. Recent scientific contributions, such as [36], experimentally investigated the robustness of RF fingerprinting techniques against spoofing attacks. They found that, independently from the chosen approach (being either raw I-Q samples or images), an attacker can defeat RF fingerprinting solutions if it injects less than $\frac{N}{2}$ samples into the flow of the samples, being N the number of I-Q samples adopted to create an image. The findings reported in our manuscript are orthogonal to such considerations on spoofing attacks. Indeed, in line with the current literature, and considering the approach presented in Sec. V-C, adversaries injecting less than $\frac{N}{2}$ samples ($N = 100,000$) are likely not to be detected. However, it is worth noting that assuming the same amount of I-Q samples of competing solutions, such as [16] and [12], our proposed DAT mitigation strategy achieves significantly higher accuracy. Indeed, our proposed solution requires less I-Q samples in order to generate reliable RF fingerprinting solutions, thus reducing the maximum number of I-Q samples that an adversary can inject without being detected. In this context, we also highlight that, at the time of this writing, adversaries have been able to inject only fully-formed packets (either replayed or fully-crafted), while on-the-fly modification of I-Q samples emitted by legitimate transmitters is out of the technological capabilities of currently-available hardware. Therefore, RF fingerprinting solutions are considered as effective and robust mainly when applied to high-bandwidth communication links, such as WiFi. For other communication technologies, e.g., Internet of Things (IoT) protocols involving low data-rates,

RF fingerprinting should be only considered as an additional layer of security and coupled with other cryptography-based solutions.

VII. CONCLUSION AND FUTURE WORK

A critical aspect in the successful deployment of Radio Frequency fingerprinting for physical-layer device authentication is to improve its reliability and robustness. In this paper, we have identified and characterized a new factor that affects the performance of RF fingerprinting, i.e., the power-cycling of the devices under test.

Our results show that power-cycling the radios has a negative impact on the performance of RF fingerprinting, suggesting that current state-of-the-art techniques cannot reliably obtain a PHY-layer model of the devices across multiple power-cycles. To mitigate such an issue, we have introduced a novel technique able to mitigate the DAT effect by pre-processing raw I-Q samples collected at the PHY layer. The samples are transformed into images and fed into a *ResNet* Convolutional Neural Network.

Through a comprehensive performance evaluation, we have proved that our approach mitigates the impact of both power-cycling and wireless channel fluctuations, resulting in an average classification accuracy of 0.85. This is a significant improvement compared to the average accuracy of approximately 0.5 obtained through state-of-the-art techniques based on raw I-Q samples. However, the variance observed in our results (smaller than competing solutions) suggests that a larger dataset may be necessary to achieve more reliable testing results. Our future work will focus on evaluating the performance of our technique with additional communication technologies and devices, as well as its robustness to distance and noise.

REFERENCES

- [1] N. Soltanieh, Y. Norouzi, Y. Yang, and N. C. Karmakar, "A Review of Radio Frequency Fingerprinting Techniques," *IEEE Journal of Radio Frequency Identification*, vol. 4, no. 3, pp. 222–233, 2020.
- [2] A. Jagannath, J. Jagannath, and P. S. P. V. Kumar, "A Comprehensive Survey on Radio Frequency (RF) Fingerprinting: Traditional Approaches, Deep Learning, and Open Challenges," *arXiv preprint arXiv:2201.00680*, 2022.
- [3] S. Abbas, Q. Nasir, D. Nouichi, M. Abdelsalam, M. Abu Talib, O. Abu Waraga *et al.*, "Improving Security of the Internet of Things via RF fingerprinting based device identification system," *Neural Computing and Applications*, vol. 33, no. 21, pp. 14 753–14 769, 2021.
- [4] T. Jian, Y. Gong, Z. Zhan, R. Shi, N. Soltani, Z. Wang, J. Dy, K. Chowdhury, Y. Wang, and S. Ioannidis, "Radio Frequency Fingerprinting on the Edge," *IEEE Transactions on Mobile Computing*, vol. 21, no. 11, pp. 4078–4093, 2021.
- [5] T. J. Bihl, K. W. Bauer, and M. A. Temple, "Feature Selection for RF Fingerprinting With Multiple Discriminant Analysis and Using ZigBee Device Emissions," *IEEE Transactions on Information Forensics and Security*, vol. 11, no. 8, pp. 1862–1874, 2016.
- [6] A. M. Ali, E. Uzundurukan, and A. Kara, "Assessment of features and classifiers for Bluetooth RF fingerprinting," *IEEE Access*, vol. 7, pp. 50 524–50 535, 2019.
- [7] G. Shen, J. Zhang, A. Marshall, and J. R. Cavallaro, "Towards scalable and channel-robust radio frequency fingerprint identification for LoRa," *IEEE Transactions on Information Forensics and Security*, vol. 17, pp. 774–787, 2022.
- [8] T. Jian, B. C. Rendon, E. Ojuba, N. Soltani, Z. Wang, K. Sankhe, A. Gritsenko, J. Dy, K. Chowdhury, and S. Ioannidis, "Deep learning for rf fingerprinting: A massive experimental study," *IEEE Internet of Things Magazine*, vol. 3, no. 1, pp. 50–57, 2020.

- [9] W. Wang and L. Gan, "Radio Frequency Fingerprinting Improved by Statistical Noise Reduction," *IEEE Transactions on Cognitive Communications and Networking*, 2022.
- [10] Z. Zhang, A. Hu, W. Xu, J. Yu, and Y. Yang, "An Artificial Radio Frequency Fingerprint Embedding Scheme for Device Identification," *IEEE Communications Letters*, vol. 26, no. 5, pp. 974–978, 2022.
- [11] J. Gong, X. Xu, and Y. Lei, "Unsupervised specific emitter identification method using radio-frequency fingerprint embedded InfoGAN," *IEEE Transactions on Information Forensics and Security*, vol. 15, pp. 2898–2913, 2020.
- [12] B. Hamdaoui and A. Elmaghub, "Deep-learning-based device fingerprinting for increased lora-iot security: Sensitivity to network deployment changes," *IEEE Network*, vol. 36, no. 3, pp. 204–210, 2022.
- [13] V. Brik, S. Banerjee, M. Gruteser, and S. Oh, "Wireless device identification with radiometric signatures," in *Proceedings of the 14th ACM International Conference on Mobile Computing and Networking*, ser. MobiCom '08. New York, NY, USA: Association for Computing Machinery, 2008, p. 116–127. [Online]. Available: <https://doi.org/10.1145/1409944.1409959>
- [14] D. H. Kwon, H. Li, Y. Chang, R. Tseng, and Y. Chiu, "Digitally equalized cmos transmitter front-end with integrated power amplifier," *IEEE Journal of Solid-State Circuits*, vol. 45, no. 8, pp. 1602–1614, 2010.
- [15] A. C. Polak and D. L. Goeckel, "Identification of wireless devices of users who actively fake their rf fingerprints with artificial data distortion," *IEEE Transactions on Wireless Communications*, vol. 14, no. 11, pp. 5889–5899, 2015.
- [16] A. Al-Shawabka, F. Restuccia, S. D'Oro, T. Jian, B. Costa Rendon, N. Soltani, J. Dy, S. Ioannidis, K. Chowdhury, and T. Melodia, "Exposing the fingerprint: Dissecting the impact of the wireless channel on radio fingerprinting," in *IEEE INFOCOM 2020 - IEEE Conference on Computer Communications*. IEEE Press, 2020, p. 646–655. [Online]. Available: <https://doi.org/10.1109/INFOCOM41043.2020.9155259>
- [17] S. Riyaz, K. Sankhe, S. Ioannidis, and K. Chowdhury, "Deep learning convolutional neural networks for radio identification," *IEEE Communications Magazine*, vol. 56, no. 9, pp. 146–152, 2018.
- [18] K. Sankhe, M. Belgiovine, F. Zhou, S. Riyaz, S. Ioannidis, and K. Chowdhury, "Oracle: Optimized radio classification through convolutional neural networks," in *IEEE INFOCOM 2019-IEEE Conference on Computer Communications*. IEEE, 2019, pp. 370–378.
- [19] K. Merchant, S. Revay, G. Stantchev, and B. Nossain, "Deep learning for rf device fingerprinting in cognitive communication networks," *IEEE Journal of Selected Topics in Signal Processing*, vol. 12, no. 1, pp. 160–167, 2018.
- [20] J. Yu, A. Hu, G. Li, and L. Peng, "A robust rf fingerprinting approach using multisampling convolutional neural network," *IEEE Internet of Things Journal*, vol. 6, no. 4, pp. 6786–6799, 2019.
- [21] L. Ding, S. Wang, F. Wang, and W. Zhang, "Specific emitter identification via convolutional neural networks," *IEEE Communications Letters*, vol. 22, no. 12, pp. 2591–2594, 2018.
- [22] S. Hanna, S. Karunaratne, and D. Cabric, "Wisig: A large-scale wifi signal dataset for receiver and channel agnostic rf fingerprinting," *IEEE Access*, vol. 10, pp. 22 808–22 818, 2022.
- [23] A. Elmaghub and B. Hamdaoui, "LoRa device fingerprinting in the wild: Disclosing RF data-driven fingerprint sensitivity to deployment variability," *IEEE Access*, vol. 9, pp. 142 893–142 909, 2021.
- [24] N. Soltani, K. Sankhe, J. Dy, S. Ioannidis, and K. Chowdhury, "More is better: Data augmentation for channel-resilient rf fingerprinting," *IEEE Communications Magazine*, vol. 58, no. 10, pp. 66–72, 2020.
- [25] A. Al-Shawabka, P. Pietraski, S. B. Pattar, F. Restuccia, and T. Melodia, "DeepLora: Fingerprinting lora devices at scale through deep learning and data augmentation," in *Proceedings of the Twenty-second International Symposium on Theory, Algorithmic Foundations, and Protocol Design for Mobile Networks and Mobile Computing*, 2021, pp. 251–260.
- [26] O. M. Gul, M. Kulhandjian, B. Kantarci, A. Touazi, C. Ellement, and C. D'Amours, "Fine-grained augmentation for rf fingerprinting under impaired channels," in *2022 IEEE 27th International Workshop on Computer Aided Modeling and Design of Communication Links and Networks (CAMAD)*, 2022, pp. 115–120.
- [27] S. Mohanti, N. Soltani, K. Sankhe, D. Jaisinghani, M. Di Felice, and K. Chowdhury, "Airid: Injecting a custom rf fingerprint for enhanced uav identification using deep learning," in *GLOBECOM 2020-2020 IEEE Global Communications Conference*. IEEE, 2020, pp. 1–6.
- [28] S. Rajendran, Z. Sun, F. Lin, and K. Ren, "Injecting reliable radio frequency fingerprints using metasurface for the internet of things," *IEEE Transactions on Information Forensics and Security*, vol. 16, pp. 1896–1911, 2020.
- [29] W. Yan, T. Voigt, and C. Rohner, "Rrf: A robust radiometric fingerprint system that embraces wireless channel diversity," in *Proceedings of the 15th ACM Conference on Security and Privacy in Wireless and Mobile Networks*, 2022, pp. 85–97.
- [30] F. Restuccia, S. D'Oro, A. Al-Shawabka, M. Belgiovine, L. Angioloni, S. Ioannidis, K. Chowdhury, and T. Melodia, "Deepradioid: Real-time channel-resilient optimization of deep learning-based radio fingerprinting algorithms," in *Proceedings of the Twentieth ACM International Symposium on Mobile Ad Hoc Networking and Computing*, 2019, pp. 51–60.
- [31] F. Restuccia, S. D'Oro, A. Al-Shawabka, B. C. Rendon, S. Ioannidis, and T. Melodia, "Deepfir: Channel-robust physical-layer deep learning through adaptive waveform filtering," *IEEE Transactions on Wireless Communications*, vol. 20, no. 12, pp. 8054–8066, 2021.
- [32] Ettus Research, "USRP X310," <https://www.ettus.com/all-products/x310-kit/>, 2020, (Accessed: 2023-Jan-03).
- [33] —, "UBX160 Daughterboard," <https://www.ettus.com/product/details/UBX160>, 2020, (Accessed: 2023-April-13).
- [34] DSP StackExchange, "Bandwidth with complex sampling," <https://dsp.stackexchange.com/questions/36927/bandwidth-with-complex-sampling>, Apr. 2017, (Accessed: 2023-April-13).
- [35] B. P. Lathi, A. S. Sedra, and M. V. Valkenburg, *Modern Digital and Analog Communication Systems*, 2nd ed. USA: Oxford University Press, Inc., 1995.
- [36] G. Oliveri, S. Sciancalepore, S. Raponi, and R. Di Pietro, "PAST-AI: Physical-layer Authentication of Satellite Transmitters via Deep Learning," *IEEE Transactions on Information Forensics and Security*, pp. 1–1, 2022.
- [37] D. Zanetti, B. Danev, and S. Capkun, "Physical-layer identification of uhf rfid tags," in *Proceedings of the Sixteenth Annual International Conference on Mobile Computing and Networking*, ser. MobiCom '10. New York, NY, USA: Association for Computing Machinery, 2010, p. 353–364. [Online]. Available: <https://doi.org/10.1145/1859995.1860035>